CHAPTER 6

Case Study - The Visualization of Left-Ventricular Deformation

This case study demonstrates how our toolkit can be used to measure and visualize left ventricular deformation in order to obtain an improved understanding of cardiac mechanics. We use as examples a left-ventricular finite element model (see subsection 3.2.8) of a healthy heart and a FE model of a heart diagnosed with non-ischemic dilated cardiomyopathy, a non-ischemic disease or defect of the heart muscle which impairs its pumping action. The disease is characterized by an enlargement of the weakened heart muscle leading to inefficient contraction of the pumping chamber and to heart failure [Maya].

The following contributions are made: we apply techniques traditionally used in solid mechanics and computational fluid dynamics to biomedical data and suggest some improvements and modifications. We obtain new insight into the mechanics of the healthy and the diseased left ventricle and we facilitate the understanding of the complex deformation of the heart muscle by novel visualizations.

In the following the strain tensor $\mathbf{E}$ is defined with respect to the material coordinates of the left-ventricular finite element model introduced in subsection 3.2.8. The normal components E_{11}, E_{22}, and E_{33} represent therefore the strains in the circumferential, longitudinal, and radial directions, respectively. This approach gives better results than obtained by using the normal components of a cylindrical strain tensor as done in [GZM97][You00].

For comparison we visualize the left ventricle of the diseased heart together with that of a healthy heart. Unless noted otherwise the images show the healthy heart on the left hand side and the diseased heart on the right hand side.

6.1 Computing Ventricular Performance Measures

The performance of the left ventricle is often specified using various length, surface and volume measures such as its systolic and diastolic volume and its ejection fraction. Using our visualization toolkit the user can specify elements, faces and parameter curves and compute their volume, area and length, respectively [Wün03b, WY03].

6.1.1 Computing Volume Measures

The volume of the heart muscle can be computed using the technique explained in subsection 5.8.2. Table 6.1 shows the myocardial volume at end-diastole and end-systole and the resulting volume reduction during contraction. In general the myocardium is considered incompressible but Denney and Prince estimate that small volume changes up to 10% occur due to myocardial perfusion [DP95]. Our results show considerably higher values for the healthy heart. A possible explanation is that the wall thickening strain appears to underestimate the actual strain. We believe this is due to the fact that thickening increases dramatically toward the endocardium (due to the nearly incompressible nature of the muscle) and the tag resolution of two or three stripes across the wall (see figure 3.10) is inadequate to capture this [You02]. As a result the computed displacements underestimate the actual tag line displacements in the endocardium and hence the computed wall thickening and the myocardial volume at end-systole are underestimated.

	ED	ES	Myocardial volume reduction
Healthy heart	217.6	159.1	26.88%
Sick heart	336.7	305.3	9.32%

Table 6.1. *Myocardial volume (in cm^3) of the healthy and the diseased left ventricle at end-diastole (ED) and end-systole (ES).*

One of the most important measures of cardiac performance is the ventricular (blood) volume and the fraction of blood ejected during contraction. In order to apply the volume computation introduced in subsection 5.8.2 the left-ventricular cavity must be modeled by finite elements. Using our toolkit we can define centroids for any four vertices on the endocardial surface with common longitudinal ξ-coordinate. Connecting these vertices to the corresponding points on the endocardial surface results in 16 finite elements for the left ventricular cavity.

Figure 6.1 and 6.2 show the finite element models of the left ventricular cavity of the healthy and the sick heart, respectively, at end-diastole and end-systole.

Using equation 5.1 we can now compute the left ventricular volumes at end-diastole (ED) and end-systole (ES). The difference of these values represents the

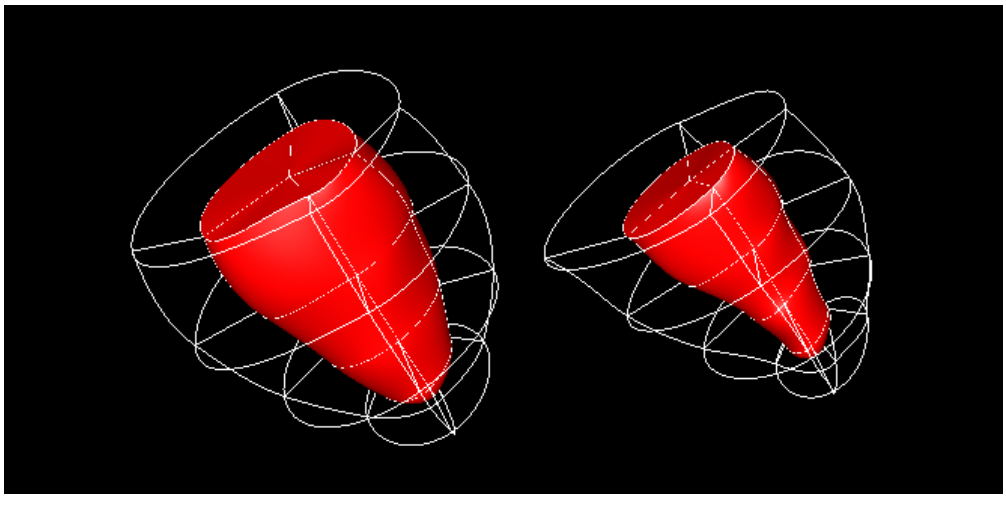

Figure 6.1. *Left ventricular cavity of the healthy heart at end-diastole (left) and end-systole (right).*

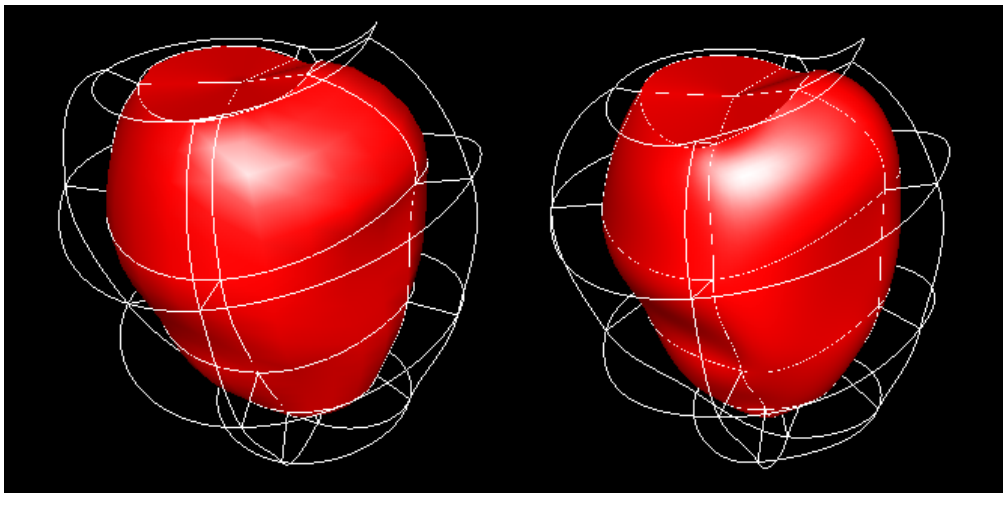

Figure 6.2. *Left ventricular cavity of the sick heart at end-diastole (left) and end-systole (right).*

stroke volume [volume of ejected blood] (SV) and the ratio of stroke volume to the volume at end-diastole represents the ejection fraction (EF). The results for the healthy and the diseased heart are shown in table 6.2.

	ED	ES	SV	EF
Healthy heart	87.15	35.08	52.07	59.75%
Sick heart	314.18	277.94	36.23	11.53%

Table 6.2. *Ventricular volume (in cm^3) of the healthy and the diseased left ventricle at end-diastole (ED) and end-systole (ES), stroke volume (SV), and ejection fraction (EF).*

The ventricular volume of the healthy heart at end-diastole is about $87cm^3$ and the stroke volume is $52cm^3$ resulting in an ejection fraction of about 60%. These values correspond well with data reported in the medical literature [Box99, LSM+02]. We think that the values slightly underestimate the actual ejection fraction due to the difficulties with computing the radial strain. The current model does not track tags at the endocardial boundary which might give a better approximation of inner wall motion.

For the diseased heart a considerable larger end-diastolic volume is observed. However, the stroke volume is only $36.23cm^3$ and about 30% smaller than for the healthy heart. The ejection fraction is only 11.5%. These values indicate a severe impairment of myocardial function.

6.1.2 Computing Ventricular Surface Areas

Table 6.3 shows the areas of the endocardial and the epicardial surface computed using equation 5.2. It can be seen that the area reduction of the sick left ventricle is severely impaired. Since the muscle fibers of the myocardium are aligned with these surfaces the measurements indicate that either muscle fibers don't contract (e.g., due to fibrosis) or that they contract in some regions but expand in other regions of the surface. In order to further examine this deformation behaviour we will visualize the strain tensor in the next section.

	ED	ES	Area reduction
Epicardial surface healthy heart	201.7	147.7	26.75 %
Endocardial surface healthy heart	93.4	53.4	42.76 %
Epicardial surface sick heart	350.6	324.6	7.40 %
Endocardial surface sick heart	218.7	200.0	8.55 %

Table 6.3. *Surface area (in cm^2) of the endocardial and the epicardial surface of the healthy and the diseased left ventricle at end-diastole (ED) and end-systole (ES).*

Using the technique introduced in subsection 5.8.2 it is also possible to compute the midventricular cavity cross-sectional area. We get as results $13.27cm^2$ at

end-diastole and $5.81cm^2$ at end-systole. From these values we determine a mid ventricular radius of $2.06cm$ at end-diastole and $1.36cm$ at end-systole which lies within the normal range of values [You02].

6.1.3 Computing Length Measures

We compute the circumference of a short-axis cross section of the left ventricular cavity by the length of a curve on the endocardial surface with a constant longitudinal ξ-parameter. The length of this curve can then be used to derive a value for the ventricular radius at that position. However, reliable results are only obtained if the arc is approximately planar and orthogonal to the long axis of the ventricle. While the technique could also be used to approximate the wall thickness at a point (by computing the arc length in radial direction) this does not necessarily yield the shortest distant between the endocardial and epicardial surface. Better computational techniques are suggested in [vR99] and alternative results are given in [KPF+99].

6.2 The Visualization of Myocardial Strain

The measurements presented in section 6.1 indicate a severe impairment of the contraction of the sick heart. In order to better understand the local deformation of the myocardium more information is required. This section presents and explains various visualizations of the strain tensor and of quantities derived from it [WY03, WLY04]. Most visualization methods in this section visualize the strain tensor by using its principal directions and principal strains explained in subsection 2.3.1.

6.2.1 Tensor Ellipsoids

As an initial visualization we display tensor ellipsoids at regular sample points throughout the midmyocardium. As explained in subsection 5.9.3 tensor ellipsoids encode the principal directions and strains by the directions and lengths, respectively, of the axes of the ellipsoid. The segments of the ellipsoids are coloured according to the sign of the principal strains with red indicating expansion and blue indicating contraction. Note that the 3D geometry is difficult to perceive from a static image. Rotating the model enables the brain to differentiate ellipsoids in the foreground and background.

Figure 6.3 shows that for the healthy ventricle the myocardium expands in the radial direction (wall thickening) and contracts in the longitudinal and circumferential direction with the circumferential contraction being in general larger. The contraction is smallest in the septum and largest in the free wall. The results correspond well with measurements reported in the literature [LOMP+94, GZM97, YICA94, DM97].

The deformation of the sick ventricle is highly abnormal. Whereas the anterior-lateral wall of the ventricle displays an almost normal deformation behaviour, albeit

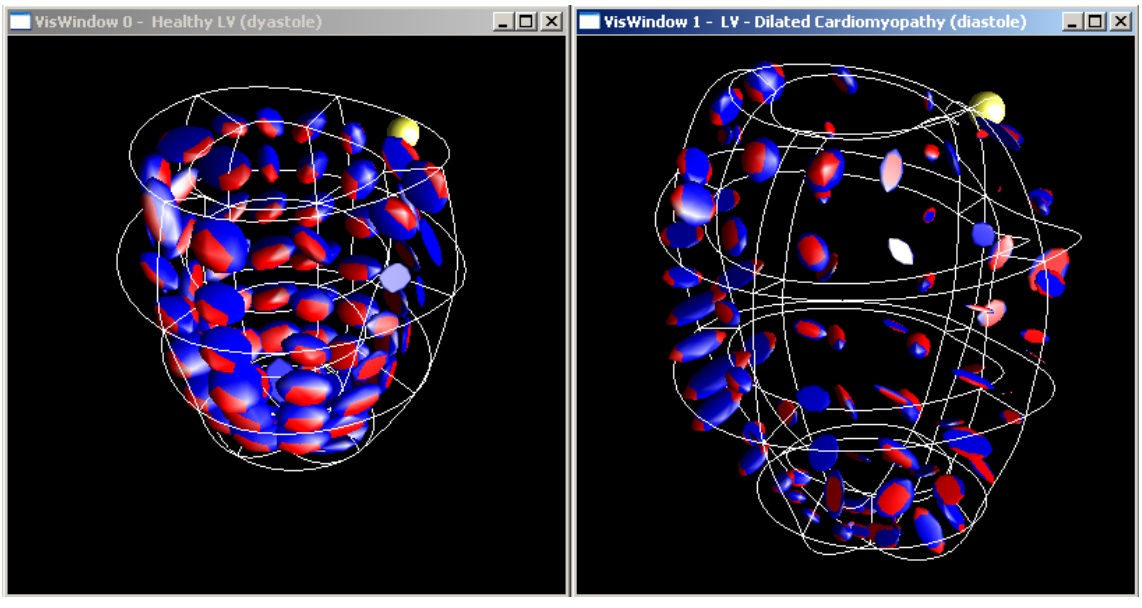

Figure 6.3. *The strain field in the midwall of the healthy (left) and the diseased (right) left ventricle visualized using tensor ellipsoids. The septal wall is indicated by a yellow sphere.*

with smaller strain values, the situation is the exact opposite in the septal wall of the ventricle. Here the myocardium is contracting in the radial direction and is expanding in the circumferential and longitudinal direction.

6.2.2 Streamlines

While each tensor ellipsoid displays the complete tensor information at a point the resulting visualization suffers from visual cluttering. A continuous representation of a vector field (e.g., an eigenvector field) along a line is obtained by using streamlines which are at each point tangential to the underlying vector field.

Figure 6.4 uses colour mapped streamlines to visualize the direction and magnitude of the major principal strain. Note that an eigenvector field is unsigned (i.e., eigenvectors have a direction but not an orientation) and that therefore the streamlines must be integrated in both the positive and the negative direction of the eigenvector field.

Streamlines are rendered as thin tubes with a constant diameter rather than as lines. Illuminating these tube-like structures gives important shape and depth cues which aid their 3D perception [WL01a]. We also render the endocardial wall (in gray) in order to reduce visual cluttering caused by the overlap of streamlines in the foreground and the background.

The image on the left of figure 6.4 shows clearly that for the healthy heart the major principal strain is oriented in the radial direction throughout the myocardial

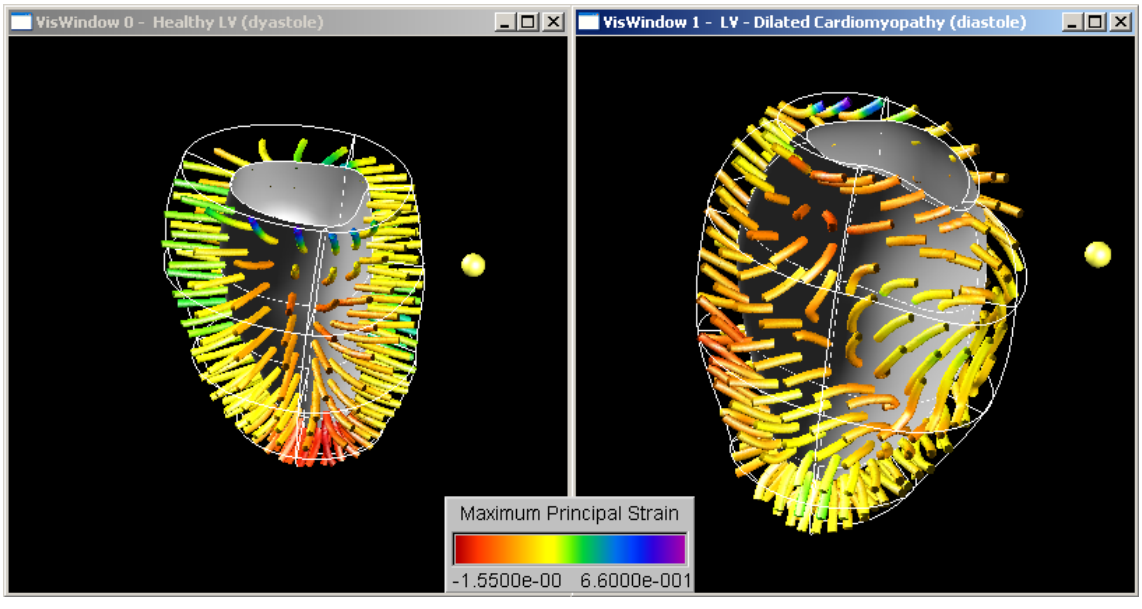

Figure 6.4. *The myocardial strain field in the healthy (left) and the diseased (right) left ventricle visualized using streamlines in the direction of the major principal strain. The septal wall is indicated by a yellow sphere.*

wall and that it is positive and increases toward the endocardium. This observation is consistent with an increased wall thickening towards the endocardium.

The image on the right of figure 6.4 confirms the previously identified abnormal contraction of the diseased left ventricle. The direction of the major principal strain is normal in the anterior-lateral and the inferior-lateral wall. However, the magnitude of the major principal strain in the inferior-lateral wall is considerably smaller than for the healthy heart and is negative in some regions (indicating a wall thinning instead of a wall thickening). In the septal wall of the diseased heart the maximum principal strain is oriented in the longitudinal and circumferential directions rather than in the radial direction.

6.2.3 Hyperstreamlines

Streamlines encode only one eigenvector. A continuous representation of the complete strain tensor along a line is achieved by using hyperstreamlines [DH93].

The trajectory of a hyperstreamline is a streamline in an eigenvector field. The other two eigenvectors and corresponding eigenvalues of the strain tensor define the axes and lengths of the ellipsoidal cross section of the hyperstreamline. The remaining eigenvalue is colour mapped onto the hyperstreamline.

Figure 6.5 and 6.6 show hyperstreamlines in the direction of the major and minor principal strain, respectively. The image on the left of figure 6.5 shows again that for the healthy heart the major principal strain is oriented in the radial direction

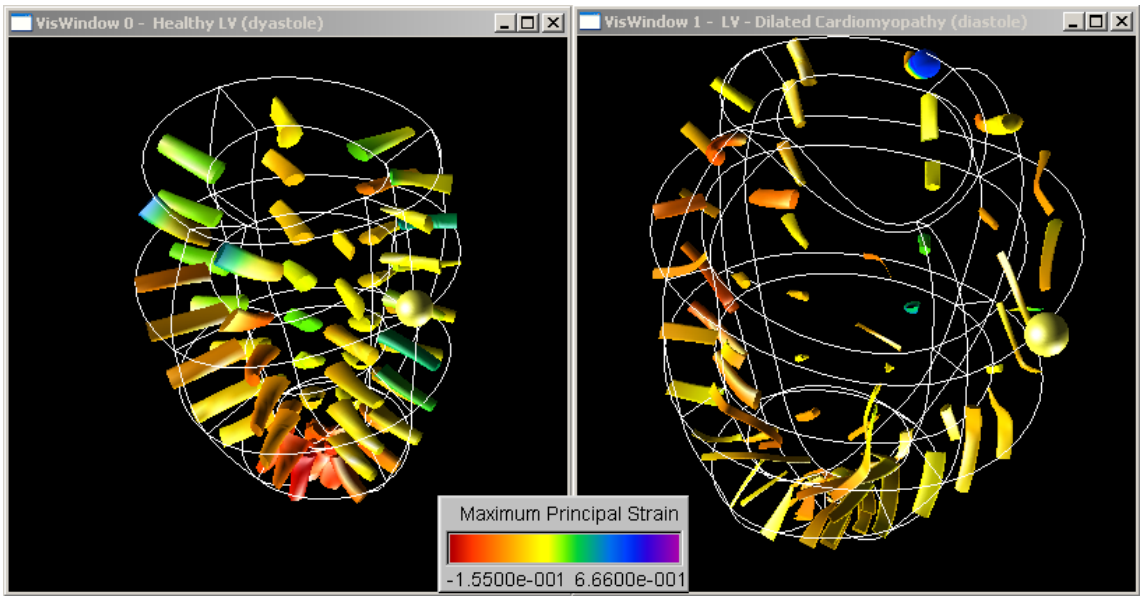

Figure 6.5. *The strain field in the healthy (left) and the diseased (right) left ventricle visualized using hyperstreamlines in the direction of the major principal strain. The septal wall is indicated by a yellow sphere.*

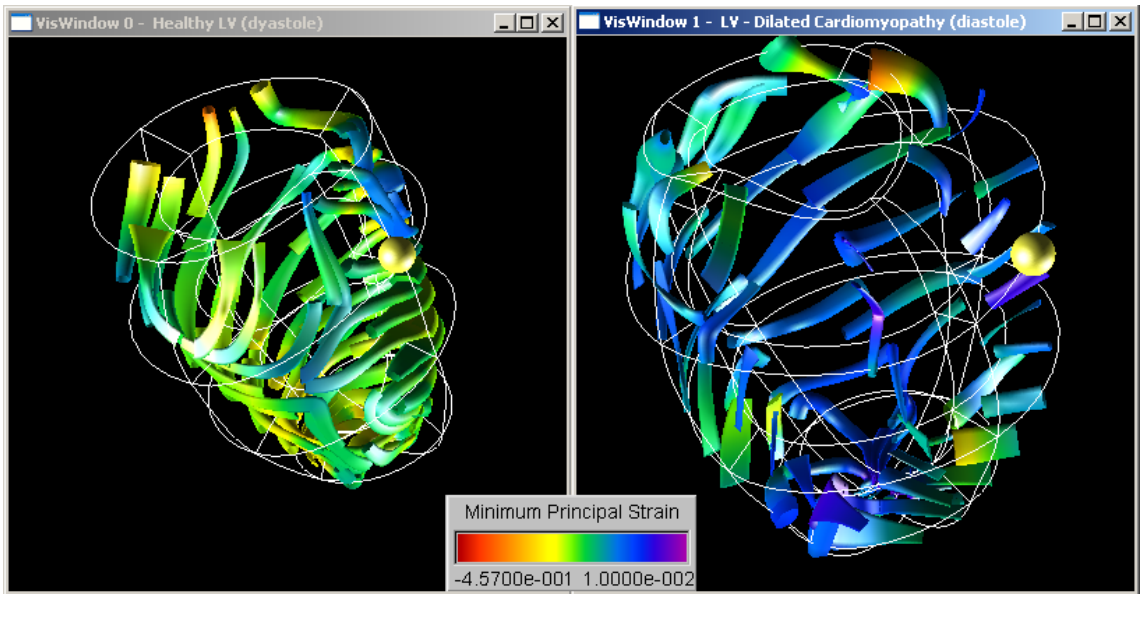

Figure 6.6. *The strain field in the healthy (left) and the diseased (right) left ventricle visualized using hyperstreamlines in the direction of the minor principal strain. The septal wall is indicated by a yellow sphere.*

throughout the myocardial wall and that it is positive and increases toward the endocardium. Furthermore it can be seen from the diameter of the cross section of the hyperstreamline that with the exception of the septal wall the magnitude of the transverse strains increases from the epicardial to the endocardial surface. We are not aware of any previous work showing all these properties with a single image.

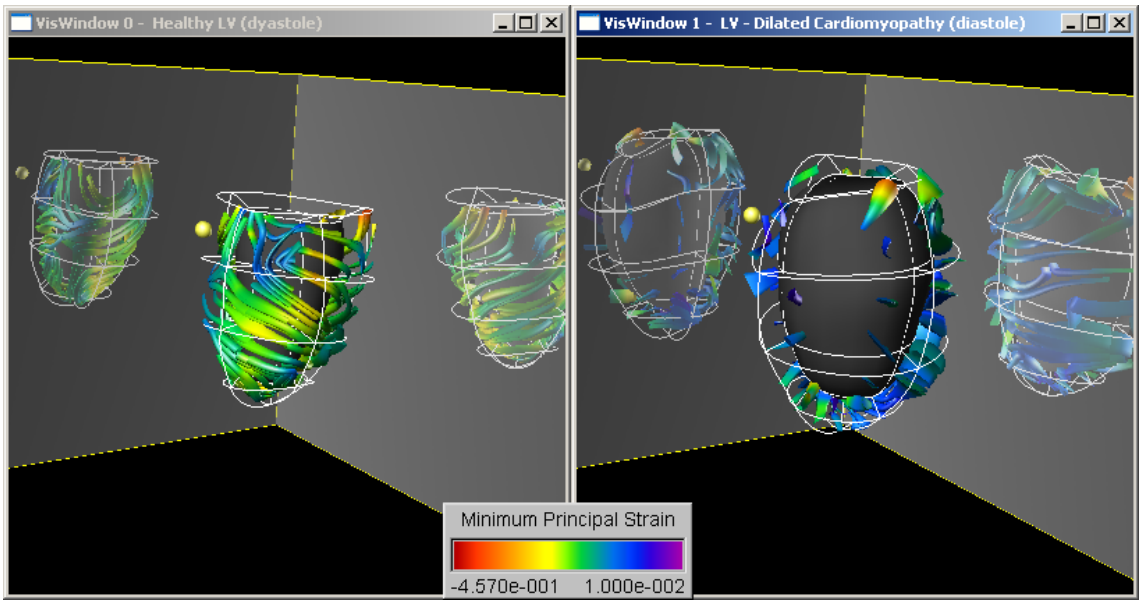

Figure 6.7. *The strain field in the healthy (left) and the diseased (right) left ventricle visualized using hyperstreamlines in the direction of the minor principal strain. Perception of the complex 3D geometry is improved by rendering the endocardial wall in gray and by inserting mirrors into the scene. The septal wall is indicated by a yellow sphere.*

The perception of the hyperstreamlines in the direction of the minimum principal strain, shown in figure 6.6, is straightforward when using an animated visualization but it is difficult when using the given figure alone. Figure 6.7 shows an improved version of this visualization. Perception is enhanced by rendering the endocardial surface in gray. The occluded portion of the visualization is revealed by using two mirrors.

The figure shows that the minimum principal strain of the healthy left ventricle is compressive throughout most of the myocardium and its direction over most of the myocardium resembles a spiral moving toward the apex. This strain direction corresponds well with the motion of the heart described in the medical literature: the septum initially performs an anticlockwise rotation (apex-base view) but later a more radial movement. The apex rotates overall anticlockwise whereas the base rotates clockwise. The anterioseptal regions of the mid and apical levels and the posterioseptal region of the base perform a hook-like motion because of a reversal of rotation [YICA94]. Note that we have in the posterioseptal region and the anterioseptal region one interesting feature where the hyperstreamlines change suddenly

their direction.

The image on the right hand side of figure 6.7 illustrates again that the minor principal strain in the lateral wall of the diseased heart (right mirror image) is similar to that of the healthy heart. In contrast to this the minimum principal strain in the septal, posterioseptal (left mirror image) and the anterioseptal wall (facing the viewer) points in the radial direction. Note that this is highly abnormal since for the healthy heart the radial direction is aligned with the direction of the maximum principal strain (see figure 6.5).

6.2.4 Line Integral Convolution

The above described features where hyperstreamlines change direction can be examined in more detail using a line integral convolution texture. We use the direction of the minor principal strain as a vector field and use its magnitude to colour map the texture.

Figure 6.8 shows that the maximum compressive strain in the midmyocardium is predominantly oriented in the circumferential direction with a slight downward tilt. Several interesting points exist where the strain suddenly changes direction. Results from tensor analysis show that these points are *degenerate points* for which at least two eigenvalues are equal [DH94]. Two such points are indicated by magenta coloured disks in the enlarged region shown on the right hand side of the top image. We found that most of the degenerate points occur on or near the septal wall. The unusual variations in strain orientation might be caused by the right ventricular wall which is connected to the left ventricular wall at both sides of the septum.

In contrast to the healthy heart the strain field of the sick heart contains considerable more degenerate points distributed throughout the myocardium. The enlargement on the right hand side of the image in the middle shows the presence of a line for which each point on it is a degenerate point. The differences are especially striking when comparing the lateral wall of the healthy and the sick left ventricle shown in the two images at the bottom of figure 6.8.

6.2.5 Colour Mapped Surfaces and Isosurfaces

We conclude this section with an examination of the distribution of the strains in the material directions. Since the strain tensor is defined with respect to the material coordinates the strains in the circumferential, longitudinal and radial directions are given by the normal components E_{11}, E_{22} and E_{33}, respectively, of the strain tensor $\mathbf{E}$.

Figure 6.9 visualizes the normal strains on the endocardial surface using colour mapping and shows additionally the 0-isosurface, which separates contracting and expanding regions. The isosurfaces were computed with the modified *Marching Cubes* algorithm described on page 172 of subsection 5.9.1.

The images on the left of the figure show clearly that the healthy left ventricle contracts in the circumferential and longitudinal directions and expands in the radial

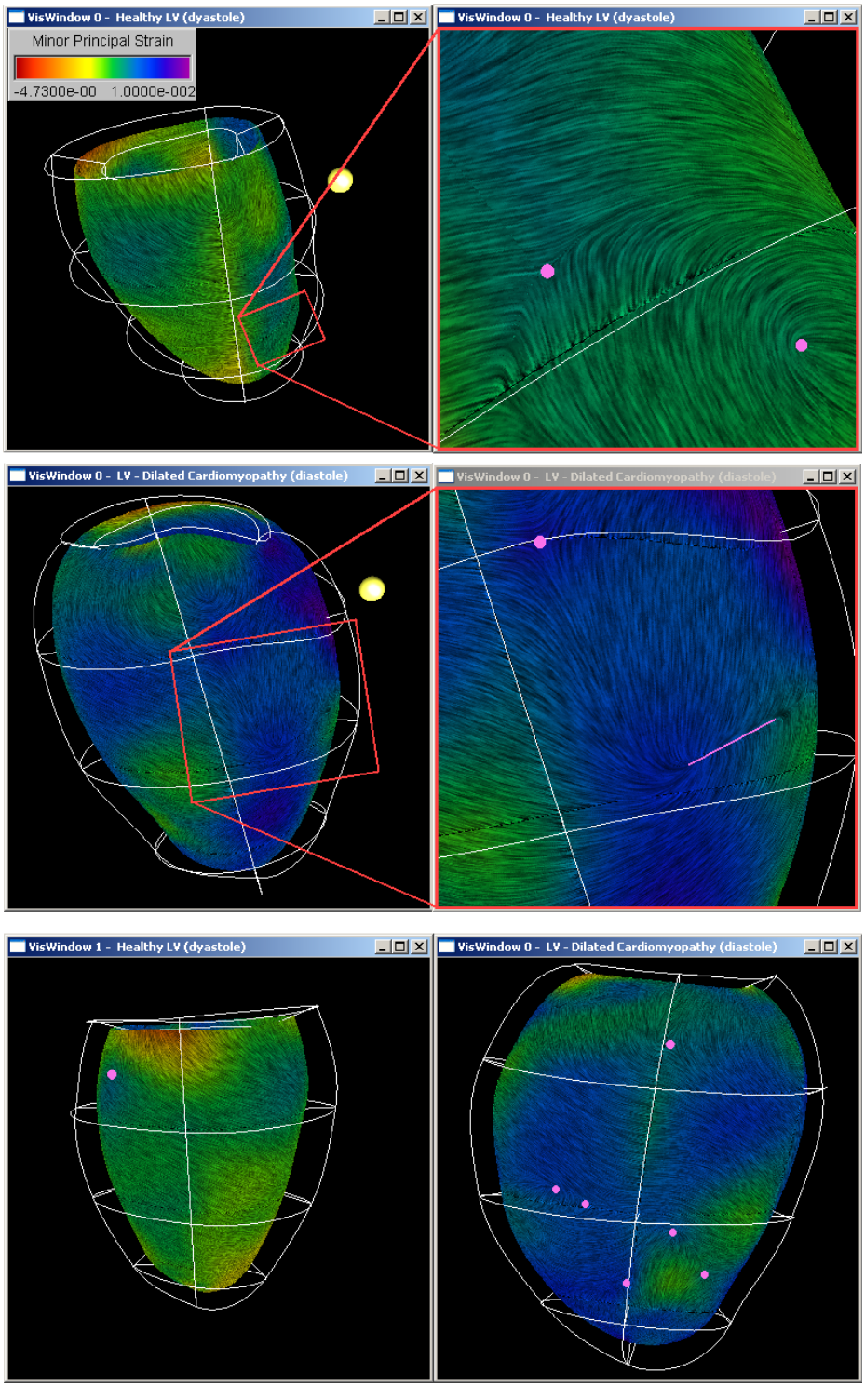

Figure 6.8. *The minor principal strain (maximum contracting strain) in the healthy (top) and the sick (middle) heart visualized using Line Integral Convolution. The bottom images show the lateral wall of the healthy (left) and the sick (right) heart. The magenta coloured disks and lines indicate degenerate points.*

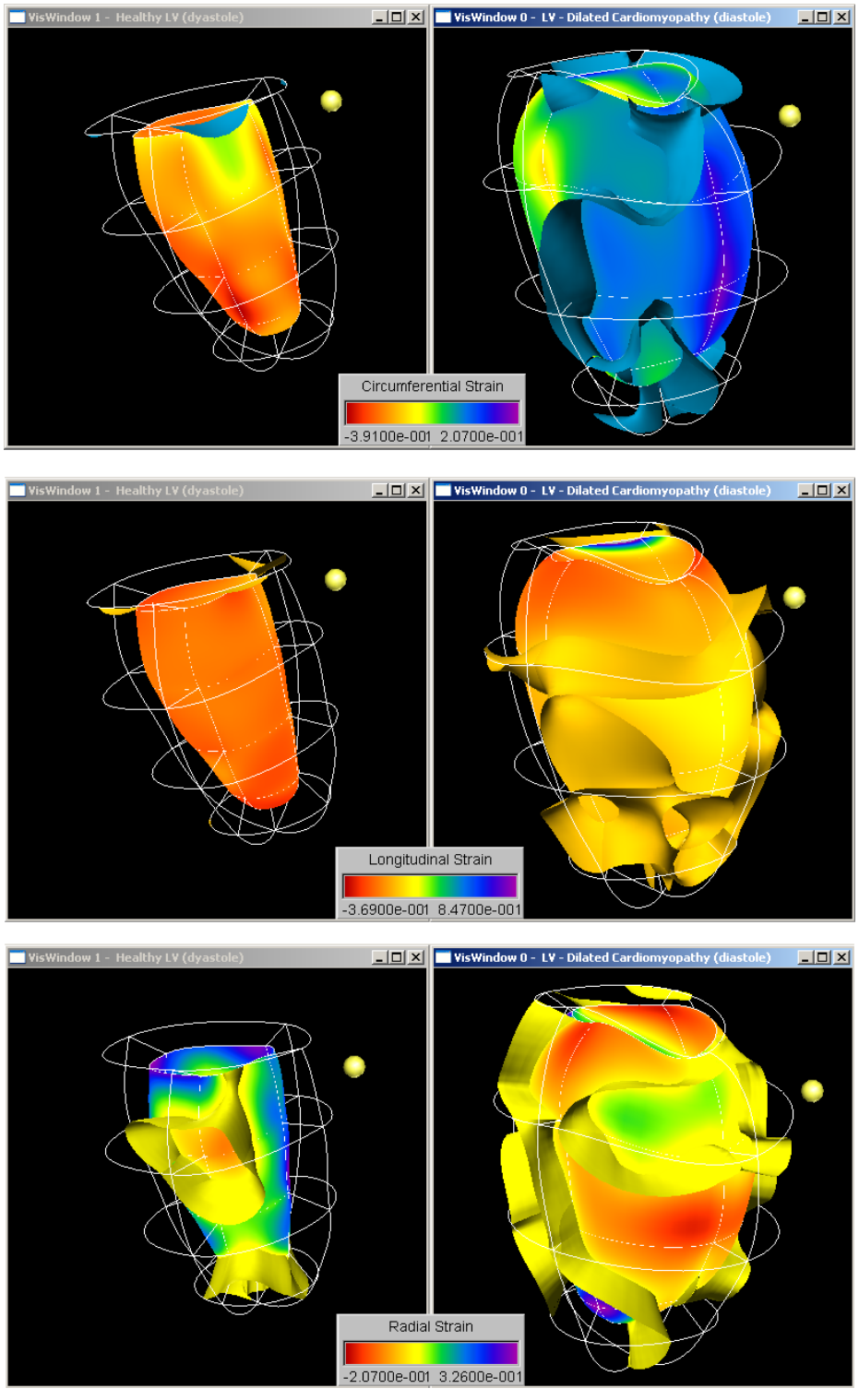

Figure 6.9. *The normal strain in the circumferential (top), longitudinal (middle) and radial (bottom) direction on the endocardial surface of the healthy (left) and the sick (right) heart visualized using colour mapping. The images show also the 0-isosurface which separates regions of contractile and expanding strain. The septal wall is indicated by a yellow sphere.*

direction. The only exceptions are some parts of the model boundary at the base and, for the radial strain, three small cylindrical regions at the apex and the septal and lateral wall. All three normal strain components are distributed relatively evenly over the endocardial surface.

For the diseased heart the lateral wall and part of the anterior and inferior wall contract in the circumferential and longitudinal directions. Wall thickening is observed in the basal-lateral wall, the basal-septal wall and in parts of the anterior and inferior wall. The rest of the myocardium shows an abnormal deformation. As a result of the strain distribution the ventricle does not contract evenly but rather performs a shape change.

We are also interested in the shear components of the strain tensor. It is known that during contraction the heart changes predominantly in diameter. LeGrice et al. [LTC95] report 8% lateral expansion but 40% wall thickening. This indicates reorganization of the myocytes during systole. Because of the sheet structure of the myocardium it has been proposed that the sheets can slide over one another restricted mainly by the length of the interconnecting collagen fibers [LTC95]. The shear properties of the myocardium resulting from this sliding motion are characterized in [DLS+00, DSYL02]. The shear is most restricted in the direction of the sheet normals and the maximum shear is possible in the fiber direction. Wall shear is thought to be an important mechanism of wall thickening during systole and therefore may play a substantial role in the ejection of blood from the ventricle.

Figure 6.10 shows a visualization of the circumferential-longitudinal shear strain (component E_{12} of the strain tensor) on the endocardial surface of the healthy (left) and the sick (right) heart visualized using colour mapping. For the healthy heart the shear strain is positive for most of the myocardium with the exception of some subepicardial regions close to the merging point with the right ventricular wall. No consistent behaviour can be found for the diseased heart. The shear in the lateral wall resembles most closely the normal range of values whereas the anterior-basal region exhibits extremely high negative strains, which might indicate impending tissue damage.

6.3 Displacement Field Visualization

The movement of the heart during contraction can be studied by visualizing the displacement field between end-diastole and end-systole. Figure 6.11 indicates the displacement at selected material points with red arrows. It can be seen that the heart moves during contraction towards the apex.

In order to analyse rotational movements we project the displacement vectors onto a radial-circumferential material plane. The results are visualized in figure 6.12 and indicate that the apex rotates overall anticlockwise (apex-to-base view) whereas the base moves in radial direction.

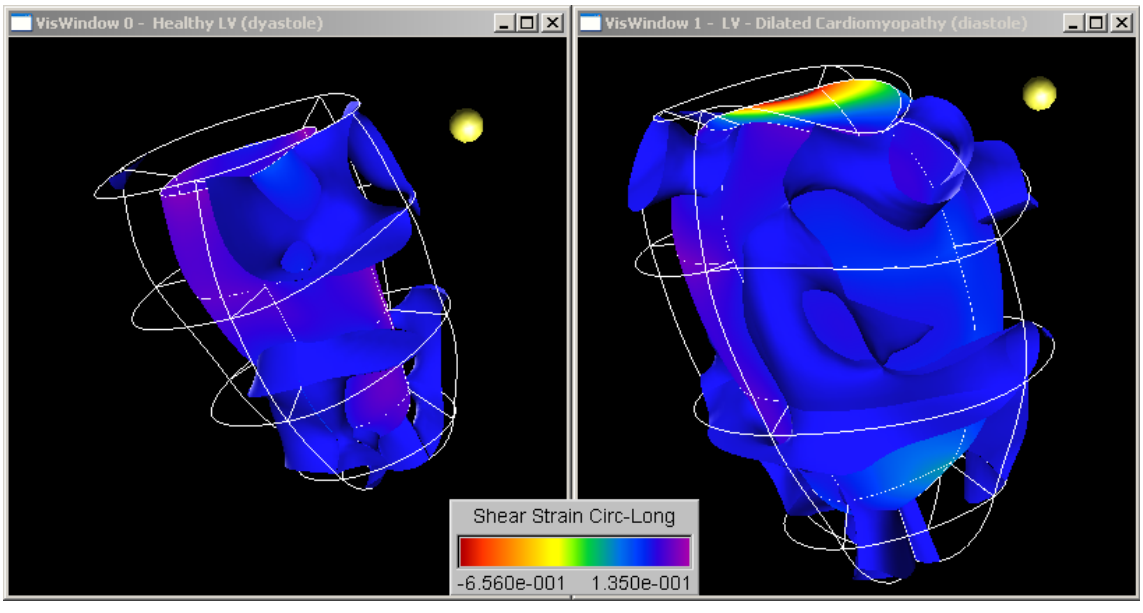

Figure 6.10. *The circumferential-longitudinal shear strain on the endocardial surface of the healthy (left) and the sick (right) heart visualized using colour mapping. The images show additionally the* 0*-isosurface of this strain component. The septal wall is indicated by a yellow sphere.*

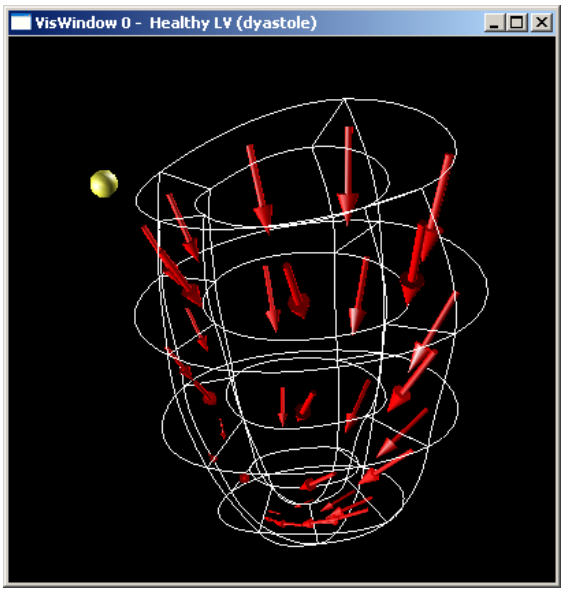

Figure 6.11. *The displacement field of the contracting left ventricle visualized using vector arrows.*

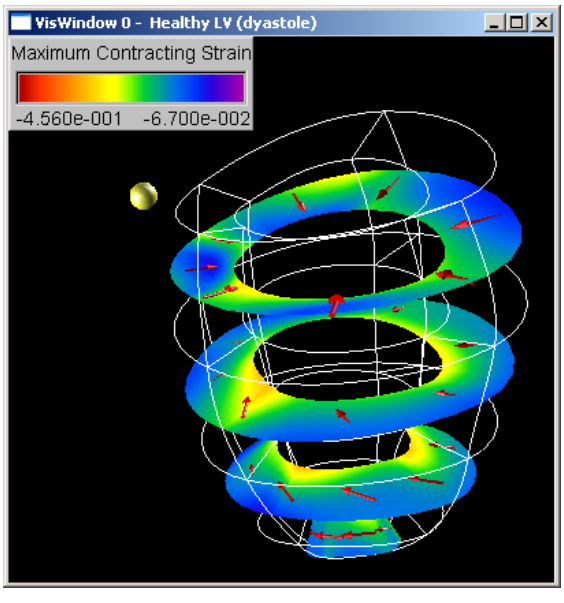

Figure 6.12. *The displacement field of the contracting left ventricle visualized using vector arrows projected onto a radial-circumferential material plane.*

6.4 Conclusion

Visualizing the strain field improves the understanding of the complex deformation of the heart muscle. Using techniques new to the biomedical field offers additional insight. The visual information can be supplemented by computing ventricular performance measures which are easily obtained from the finite element model using numerical integration.

The visualization of the healthy heart confirms observations previously reported in the literature. Using tensor ellipsoids, streamlines and hyperstreamlines makes it possible to visualize complex deformation behaviour in a single image. Line integral convolution uncovers the presence of degenerate points at which the principal strains suddenly change direction. Further investigations are necessary to find the relationship between degenerate points, fiber structure, and the ventricular anatomy. Furthermore we want to explore their significance (if any) for diagnosing heart diseases.

Visualizing a ventricle with dilated cardiomyopathy showed that the deformation of the lateral wall is roughly like that of a normal heart whereas the septal wall behaved almost in the opposite manner. Very large negative shear strains were recorded in the anterior-basal wall of the ventricle. The combined effect of these deformations seems to be a pumping action by shape deformation (from a circular to an ellipsoidal cross section) rather than by contraction.

The visualizations and measurements performed in this case study demonstrate the usefulness of our visualization toolkit for exploring biomedical models. Using the unique field data structure enables the interactive definition of new measures and facilitates the exploration of the data set. The modular OO-design allows comparison of multiple models, which is further enhanced by the user interface for colour map design and control.

6.5 Future Research

We are interested in visualizing other data sets of diseased hearts, in particularly models of ischemic myocardium. It is known that small changes in the deformation behaviour of the myocardium occur before the first symptoms of a cardiac infarct develop and we hope that visualizing myocardial strain supports the detection of regions of low blood perfusion. Non-traditional visualization methods such as hyperstreamlines, LIC and tensor topology seem to be particularly promising for this purpose.

Of particular interest is the relationship between myocardial strain and fiber structure. Recent research suggests that the measurement of the fiber structure is possible using diffusion tensor imaging [SHS+01, MFE+01, ACCM01]. Further information could be provided by fusing our data with functional data obtained by PET and SPECT [RdB99].

Of additional interest is the comparison of the myocardial deformation with the blood flow pattern in the coronary vessels. Earlier work by Kilner et al. [KYW+00]

visualized the blood flow on each MRI plane using streamlines. The authors suggest that the asymmetries and curvature of the heart have potential fluid dynamic advantages and show an improved ventriculo-atrial coupling if compared with a simpler atrio-ventricular arrangement as found in snails. It has been shown that atherosclerotic plaques develop in regions where flow rate and shear strain are relatively low and that regions of low shear strain are pathologically prone to vessel wall thickening and thrombosis [Bro00b].

We hope that in future visualizing different cardiac data sets simultaneously will further improve the understanding of the heart and the diagnosis and treatment of cardiovascular diseases.